

1 **(Revision 2)**

2 **Magnetite plaquettes are naturally asymmetric materials in meteorites**

3 Queenie H. S. Chan<sup>1</sup>, Michael E. Zolensky<sup>1</sup>, James E. Martinez<sup>2</sup>, Akira Tsuchiyama<sup>3</sup>, and Akira  
4 Miyake<sup>3</sup>

5 <sup>1</sup>ARES, NASA Johnson Space Center, Houston, Texas 77058, USA.

6 <sup>2</sup>Jacobs Engineering, Houston, Texas 77058, USA.

7 <sup>3</sup>Graduate School of Science, Kyoto University, Kitashirakawa Oiwake-cho, Sakyo-ku, Kyoto  
8 606-8502, Japan.

9

10 Correspondence to: Queenie H. S. Chan. Correspondence and requests for materials should be  
11 addressed to Q.H.S.C. (Email: [hschan@nasa.gov](mailto:hschan@nasa.gov))

12

13

**Abstract**

14 Life on Earth shows preference towards the set of organics with particular spatial configurations.

15 Enantiomeric excesses have been observed for  $\alpha$ -methyl amino acids in meteorites, which

16 suggests that chiral asymmetry might have an abiotic origin. A possible abiotic mechanism that

17 could produce chiral asymmetry in meteoritic amino acids is their formation under the influence

18 of asymmetric catalysts, as mineral crystallization can produce spatially asymmetric structures.

19 Although magnetite plaquettes have been proposed to be a possible candidate for an asymmetric

20 catalyst, based on the suggestion that they have a spiral structure, a comprehensive description of

21 their morphology and interpretation of the mechanism associated with symmetry-breaking in

22 biomolecules remain elusive. Here we report observations of magnetite plaquettes in

23 carbonaceous chondrites (CCs) which were made with scanning electron microscopy and  
24 synchrotron X-ray computed microtomography (SXRCT). We obtained the crystal orientation of  
25 the plaquettes using electron backscatter diffraction (EBSD) analysis. SXRCT permits  
26 visualization of the internal features of the plaquettes. It provides an unambiguous conclusion  
27 that the plaquettes are devoid of a spiral feature and, rather that they are stacks of individual  
28 magnetite discs that do not join to form a continuous spiral. Despite the lack of spiral features,  
29 our EBSD data show significant changes in crystal orientation between adjacent magnetite discs.  
30 The magnetite discs are displaced in a consistent relative direction that lead to an overall  
31 crystallographic rotational mechanism. This work offers an explicit understanding of the  
32 structures of magnetite plaquettes in CCs, which provides a fundamental basis for future  
33 interpretation of the proposed symmetry-breaking mechanism.

34

35

### **Keywords**

36 Magnetite, plaquettes, carbonaceous chondrites, symmetry-breaking, scanning electron  
37 microscopy, SEM, electron backscatter diffraction, EBSD, synchrotron X-ray computed  
38 microtomography, SXRCT, aqueous alteration, crystal structure

39

40

### **Introduction**

41 Magnetite ( $\text{Fe}_3\text{O}_4$ ), present in most carbonaceous chondrites (CCs), has been shown to be an  
42 effective catalyst for the formation of the amino acids that are commonly found in these same  
43 meteorites (Pizzarello 2012). Magnetite sometimes takes the form of ‘plaquettes’, or ‘platelets’,  
44 first described by Jedwab (1967). This form consists of barrel-shaped stacks of magnetite discs

45 with an apparent feature of dislocation-induced spiral growth that seem to be connected at the  
46 center, thus resembling a spiral. Although magnetite plaquettes have been studied for over 50  
47 years, and the spiral morphology of magnetite has been assumed in many studies (Jedwab 1971;  
48 Hua and Buseck 1998), a widely accepted description of the structure and morphology of this  
49 particular magnetite form is lacking. However, a detailed description is necessary in order to  
50 confirm or disprove the spiral configuration.

51

52 Magnetite plaquettes have been found in various CCs, typically in the most carbon-rich CI  
53 (Ivuna-like) chondrites, and also in the CR (Renazzo-like) chondrites, ungrouped type 2  
54 carbonaceous chondrites (C2s) Tagish Lake and Essebi, and sometimes in unusual CM (Mighei-  
55 like) chondrites (for example, Bells; M. Zolensky, personal communication) (Weisberg et al.  
56 1993; Zolensky et al. 1996b; Hua and Buseck 1998; Zolensky et al. 2002; Greshake et al. 2005).  
57 Magnetite does not occur as plaquettes in meteorites from other chondrite classes (e.g., CO, CV,  
58 CK etc.) which show little or no aqueous alteration. The only report of magnetite plaquettes in a  
59 CV chondrite was for CV2 MIL 090001 (Keller and Walker 2011), which was later re-classified  
60 as a CR2 chondrite based on its whole rock oxygen isotopic composition (Keller et al. 2012).  
61 Magnetite was originally suggested to have formed as a condensate from nebular vapor (Jedwab  
62 1967). However, Kerridge et al. (1979) proposed that the platy morphology of magnetite  
63 plaquettes is controlled by nucleation during aqueous alteration on a parent body. A similar  
64 conclusion was drawn by Bradley et al. (1998), who observed similar epitaxial growth of  
65 magnetite with secondary carbonates. Magnetite in these chondrites often replaces Fe sulfides  
66 (Zolensky et al. 1996a; Lipschutz et al. 1999; Trigo-Rodriquez et al. 2013), frequently as

67 pseudomorphs. For example, magnetite framboids replace euhedral pyrrhotite in Tagish Lake,  
68 indicating late stage oxidation (Zolensky et al. 2002; Izawa et al. 2010). Framboidal and acicular  
69 magnetite also occurs adjacent to pyrrhotite, and the crystal relationship indicates that the  
70 pyrrhotite was being gradually consumed by secondary, aqueous fluids which produced the  
71 magnetite.

72

73 Molecular asymmetry in the form of L-enantiomeric excess (*Lee*) has been observed for amino  
74 acids in meteorites, and L-homochirality is also common to all terrestrial life forms. The possible  
75 spiral configuration of individual magnetite plaquettes could have provided a naturally  
76 asymmetric scaffold, from which the asymmetry could be inherited by reactions and syntheses to  
77 the adsorbed organic molecules (Pizzarello and Groy 2011). Despite their occurrence in  
78 extraterrestrial materials, magnetite plaquettes are apparently absent from terrestrial  
79 environments. If the magnetite plaquettes are naturally asymmetric, this underscores the  
80 significance of an extraterrestrial source of asymmetric components, of which the asymmetry  
81 could have been amplified through other processes occurring on Earth or the asteroidal parent  
82 body. In order to understand the distribution of ‘spiral’ magnetite among different meteorite  
83 classes, as well as to investigate their spiral configurations and possible correlation to molecular  
84 asymmetry, we observed polished thin sections of CCs using scanning electron microscopy  
85 (SEM) to locate well-exposed plaquettes. These plaquettes were then examined using  
86 synchrotron X-ray computed microtomography (SXRCT) and electron backscatter diffraction  
87 (EBSD) in order to understand their internal structure and reconstruct the crystal orientation  
88 along the stack of magnetite discs.

89

90

## Methods

91

We analyzed polished thin sections of fifteen CCs spanning different classes – **CI1**: Alais

92

(USNM 6659-9), Ivuna (AMNH 3963 MZ1), Orgueil (FM ME509 MZA1, 2, 4); **CM1**: MET

93

01070,8, LAP 02422,1; **shocked CM1**: Bench Crater (a CC found in lunar regolith sample

94

12037,188); **CM2**: Murchison (FM ME5449 MZ1), Mighei (FM ME1456 MZ2); **CO3**:

95

ALHA77307,39; **CV3**: NWA 2086 (MZ1) (reduced) (Kereszturi et al. 2014); **CR1**: GRO

96

95577,3; **CR2**: GRA 95229,19, Renazzo 6 (FM ME5996 MZ6); **CH3**: PCA 91467,15; **C2-**

97

**ungrouped**: Tagish Lake (MG62-1).

98

99

Backscattered electron (BSE) imaging and mineral elemental compositions were obtained using

100

the JEOL 7600F Field Emission Scanning Electron Microscope (FE-SEM) at the E-beam

101

laboratory of the Astromaterials Research and Exploration Science (ARES) organization, NASA

102

Johnson Space Center (JSC). We performed a systematic scanning of the thin sections. BSE

103

images were acquired using a low-angle backscattered electron (LABE) detector with an

104

accelerating voltage of 20 kV and beam current of 15 nA. The SEM system was coupled to a

105

Thermo Fisher Scientific energy-dispersive spectrometry (EDS) X-ray detector with NORAN

106

System Seven (NSS) microanalysis software (Version 3.0). Magnetites were identified with

107

reference to their morphology and EDS spectra using the NSS Point and Shoot mode.

108

109

EBSD maps were collected with the use of a Zeiss SUPRA 55VP FE-SEM with a Bruker

110

Quantax CrystAlign 400i EBSD system coupled with a Bruker  $e^-$ Flash EBSD detector at the

111 Structural Engineering Division, NASA JSC. Prior to the EBSD analysis, the carbon coating  
112 needed for SEM analysis was removed by mechanical polishing with 0.05  $\mu\text{m}$  colloidal silica on  
113 a Buehler EcoMet variable speed grinder-polisher with a final polishing wheel utilizing a porous  
114 neoprene Struers MD-Chem polishing pad. The thin sections were rinsed with deionized water  
115 and dried with nitrogen in order to remove any polishing residue. The polished thin sections were  
116 attached to a sample holder with ElectroDag (Ted Pella, Inc.) to prevent sample movement, and  
117 the vaporized mounting chemicals were evacuated in a vacuum bell jar at  $10^{-5}$  torr for 1 hour.  
118 The final polishing and sample mounting procedures are essential for optimal EBSD operations.

119

120 For EBSD, a single crystal silicon wafer with a [110] type reference direction was used as a  
121 standard for system calibration prior to sample analysis. The SEM parameters were: Accelerating  
122 voltage – 20 kV; Aperture – 120  $\mu\text{m}$  (largest); High current mode – on; Beam size –  
123 approximately 3 to 5 nm; Incident beam current – 9.2 to 9.3 nA; Magnification – 9590 $\times$ ;  
124 Chamber Pressure in Variable Pressure Mode – 45 Pa; Working distance – 20.5 mm. The EBSD  
125 parameters were: Band Detection – 7 bands (max.); Detector Distance – 15.87 mm (fully  
126 inserted); Detector Tilt – 3.3 $^{\circ}$ ; Imaging system – 1024  $\times$  768; Pixel Size – 57 nm; Raster – 5  $\times$  5.  
127 The EBSD patterns were analyzed with a reduction software associated with the Bruker EBSD  
128 system.

129

130 The region of interest (ROI) for focused ion beam (FIB) preparation and SXRCT analysis was  
131 selected based on FE-SEM observation of the Orgueil sample where magnetite plaquettes were  
132 abundant and their morphology was less disrupted by mechanical polishing. To protect the

133 particle surface from ion beam damage, the surface was coated with an approximately 20-nm-  
134 thick carbon layer. Then, the particle surface was coated by electron beam-deposited Platinum  
135 (Pt) followed by a Ga ion-deposited Pt layer at Kyoto University. A parallelepiped-shaped  
136 sample (~35×30×20 μm in size) was removed from the thin section by a FIB-SEM (FEI Quanta  
137 200 3DS) at Kyoto University using a Ga ion operated at 30 kV with beam currents ranging from  
138 3 nA to 30 nA. Then, the section was attached to a thin W-needle and imaged by a SR-based  
139 imaging microtomography system with a Fresnel zone plate at the SPring-8 BL47XU beamline,  
140 Hyogo, Japan. The sample was imaged at 7 and 8 keV for identification of minerals (Tsuchiyama  
141 et al. 2013). The computed tomography (CT) images with voxel (pixel in 3-D) size of 34.6 nm  
142 (effective spatial resolution of was approximately 200 nm) were reconstructed from 1800  
143 projection (rotation of 0.1° per projection) images using a convolution back-projection algorithm.  
144 The final compiled three-dimensional structure was obtained by stacking successive CT images.

145

## 146 **Results and discussion**

### 147 **General morphology of magnetite plaquettes observed by SEM**

148 Among the fifteen CCs we examined, magnetite plaquettes have previously been reported as  
149 being abundant in Orgueil (Jedwab 1967), Renazzo (Weisberg et al. 1993), and Tagish Lake  
150 (Zolensky et al. 2002; Greshake et al. 2005). In this study, magnetite plaquettes were observed in  
151 nine CC samples (Alais, Ivuna, Orgueil, LAP 02422, GRO 95577, GRA 95229, Renazzo, PCA  
152 91467, and Bench Crater) (**Figure 1**, Supplementary **Figure S1**). CIs generally have higher  
153 abundances of magnetite plaquettes, followed by CRs, while CHs and CMs rarely contain  
154 magnetite plaquettes. We can summarize that the approximate, observed abundance of magnetite

155 plaquettes follows the sequence of  $CI1 > CR1 = CR2 > CM1 \geq CH3$ , while we did not locate  
156 magnetite plaquettes in CM2, CO3, or CV3. The magnetite plaquettes are 5 to 16  $\mu\text{m}$  in size  
157 (**Figure 1** and **Table 1**). The measurements generally agree with the data reported for Orgueil (a  
158 few to tens of micrometers) by Hua and Buseck (1998). Magnetite plaquettes are commonly  
159 observed as clusters as well as individual grains. Framboidal magnetite grains usually occur  
160 around the magnetite plaquettes (**Figure 1d**), while in some cases the magnetite framboids leave  
161 indentations on the surface of the plaquettes after the framboid grains were plucked from  
162 sections. Their coexistence suggests contemporary crystallization of the two forms of magnetite.  
163 Other than isolated spherules, framboids and plaquettes, we have also observed a “cabbage-like”  
164 morphology that has not been previously described for the CC magnetite (Supplementary **Figure**  
165 **S2**).

166

### 167 **Magnetite and parent body aqueous alteration processes**

168 The occurrence of magnetite plaquettes in CCs appears to correlate with (1) chondrite group and  
169 (2) extent of aqueous alteration that the meteorite sample has undergone. Magnetite plaquettes  
170 are more commonly found in chondrites which show a significant degree of aqueous alteration  
171 (petrologic type 1 chondrites from the CI, CR and CM groups). They are abundant in CI  
172 meteorites which occur only as petrologic type 1 chondrites, and which comprise the most  
173 aqueously altered group of meteorites. Although they are also observed in some type 2  
174 meteorites (only in the CR2s GRA 95229 and Renazzo but none were observed in the CM2  
175 meteorites analyzed in this study), their occurrence there is rare. No magnetite plaquettes were  
176 found in the type 3 chondrites which have undergone very limited or no aqueous alteration,

177 except for CH3 PCA 91467. Although PCA 91467 is classified as a type 3 chondrite, it was  
178 shown to resemble type 1-2 chondrites in terms of the presence of heavily hydrated type 1 and  
179 type 2 clasts and amino acid content (Sugiura 2000; Burton et al. 2013). We could not find  
180 magnetite plaquettes in the Murchison and Mighei samples, although it is premature to conclude  
181 that magnetite plaquettes are completely absent from these meteorites due to the small number of  
182 thin sections studied and the typically brecciated and heterogeneous natures of these meteorites.

183

184 Magnetite plaquettes usually occur along healed fractures (**Figure 1b**) and also as dispersed  
185 grains in the meteorite matrix, and they are often associated with or contained within carbonates,  
186 such as calcite and dolomite, and phyllosilicates (**Figure 1**), all of which are of aqueous origin  
187 and must therefore have formed on a parent body (especially when situated inside of cracks)  
188 (Kerridge et al. 1979). The association with carbonates is more commonly observed for the  
189 euhedral trapezohedral form of magnetite crystals, which is another typical form of magnetite  
190 occurring as framboids. The magnetite plaquettes are purely iron oxide rather than including  
191 other elements of similar ionization potentials (e.g. Co, Cu, Ni), which suggest that the magnetite  
192 plaquettes are unlikely to have formed by condensation from nebular vapor. Formation of  
193 magnetite controlled solely by crystal structure can produce close-packed (111) planes (Bennett  
194 et al. 1972) that exhibit three- or pseudo-sixfold symmetry. However, only a fourfold symmetry  
195 has been observed for magnetite plaquettes (Jedwab 1971). Kerridge et al. (1979) suggested that  
196 the fourfold symmetry could indicate that the magnetite discs belong to {100} planes, as their  
197 formation were controlled by the microenvironment as defined by the oxygen networks of the  
198 associated carbonate structure. This possible epitaxial relationship is supported by the frequent

199 magnetite-carbonate association, however such a relationship is not universal and thus the  
200 hypothesis should be revisited in a future study. Our EBSD observations are in agreement with  
201 their interpretations in that the planar surfaces of the magnetite discs belong to the  
202 crystallographic {100} faces (see section “Possible rotational feature as observed by EBSD  
203 analysis”).

204

### 205 **Are magnetite plaquettes spirals?**

206 One reason magnetite plaquettes have drawn decades of attention is the striking appearance of  
207 the “spiral” morphology that suggests formation by dislocation-induced crystal growth (Jedwab  
208 1971). The apparent spiral feature with a possible hollow core was documented by Jedwab  
209 (1971), and apparently supported by a later high-resolution imaging study that showed a curved  
210 twist on the terminating plates of the magnetite stack (Hua and Buseck 1998). However, Sheldon  
211 and Hoover (2012) noted that the final plate in a stack is prone to damage and thus the spiral  
212 feature might not be intrinsic.

213

214 Our images show that the terminating plates of the plaquettes sometimes show an apparent twist,  
215 or adjacent plates appearing to be joined by a spiral bridge (**Figure 1c** and Supplementary  
216 **Figure S5**). However, these are likely laboratory-induced features caused by mechanical  
217 polishing during thin section preparation. On the contrary, **Figure 1d** and Supplementary **Figure**  
218 **S6** show that the surfaces of the terminating plates are smooth and clearly devoid of the spiral  
219 features used to substantiate the spiral morphology in previous studies (Jedwab 1971; Hua and  
220 Buseck 1998). The magnetite plates are either tilted sideways or protected by adjacent features

221 so that the surfaces are less susceptible to the polishing effect, and thus they better retain and  
222 represent the original morphology. The plaquettes do not have a hollow core as assumed in  
223 previous studies, instead they occur as separate discs with a solid center in each disc. Defect  
224 structures represented by a helicoid (or spiral ramp) and a dislocation core that are typical in  
225 screw dislocation are also absent in the magnetite plaquettes, therefore the magnetite discs are  
226 formed by nucleation of multiple discs (Meunier 2006), and the rotation is controlled by  
227 interlayer electrical interactions/magnetism, rather than continuous crystal growth by dislocation.  
228 Our observation is in agreement with the description given by Sheldon and Hoover (2012) that  
229 the magnetite plates did not appear to be attached to each other. However, their suggestion that  
230 the plates were held together by an exterior membrane was not confirmed in our study. We  
231 observed no such membranes.

232

233 We also collected SXRCT images of the magnetite plaquettes in an Orgueil FIB section to obtain  
234 their three-dimensional internal structures (**Figure 2**). The computed tomography (CT) images  
235 unambiguously show that the plaquettes do not show any spiral features but rather are stacks of  
236 nearly parallel discs. Our SXRCT observations also indicate that the plaquettes do not have a  
237 hollow core, instead each disc shows an explicit solid center. We note that there is an apparent  
238 central column in **Figure 2b**. Such a “column” represents the thicker inner regions of the  
239 magnetite discs which are tightly packed, but they are not connected. According to dislocation  
240 theory, surface dislocation features (typically nanometer scale) can be described by the Burgers  
241 vector, and thus are a function of the dimensions of the crystal lattice and the amount of slip  
242 (Frank 1949). Such localized small-scale surficial dislocation steps are not observable by the

243 SXRCT resolution (34.6 nm; effective spatial resolution of ~200 nm). Nevertheless, the absence  
244 of a helicoid and the variation in the crystal orientations of the magnetite discs unambiguously  
245 show that the plaquettes are not formed by a screw dislocation, which would lead to localized  
246 distortion and consistent crystal orientation throughout the stack. We discuss this further in the  
247 following section.

248

### 249 **Possible rotational feature as observed by EBSD analysis**

250 We further analyzed the crystallography of magnetite plaquettes by EBSD. Orgueil was chosen  
251 for EBSD analysis because of the high abundance of magnetite plaquettes in the sample. An  
252 example of the crystal structure and calculated EBSD patterns for magnetite are shown in **Figure**  
253 **3**, and the location of this spot is marked by yellow crosses on **Figure 4a and b**. The observed  
254 pattern was matched to a calculated magnetite pattern that indicates the local crystallographic  
255 orientation for the analyzed spot (**Figure 4a**). The corresponding crystal orientations are  
256 represented by the inverse pole figure (IPF) map shown in **Figure 4b**, where areas of the same  
257 color share the same crystal orientation.

258

259 EBSD reveals that the magnetite crystal orientation is consistent within a single magnetite disc.  
260 As seen in **Figure 4c**, the crystal orientation changes less than  $6^\circ$  in a disc, which indicates that  
261 each magnetite disc was formed as a single crystal with one preferred crystal orientation. The  
262 planes of the discs belong to the  $\{100\}$  planes of the cubic inverse spinel space group. Although  
263 spiral dislocation-induced crystal growth can also result in  $[100]$  vertical propagation forming  
264 crystals of essentially a single orientation (Yao et al. 2009), such consistency in crystal

265 orientation was not observed between different discs in a magnetite stack, where the crystal  
266 lattice clearly rotates from one disc to another. This results in a striking color variation as shown  
267 in the IPF maps (**Figure 4b**), and the notable range of misorientations (5–35°) between discs  
268 along the profile of a magnetite plaquettes (B–B”) as shown in **Figure 4d**.

269

270 Significant changes in crystal orientation are observed *between* adjacent magnetite discs (**Figure**  
271 **4**). Therefore, although individual discs are not connected as a continuous spiral, variation in  
272 crystal orientation across the magnetite stack provides a mechanism for a rotational relationship  
273 at the molecular level. We studied the extrapolated crystal orientation figure of each magnetite  
274 disc (similar to the figure shown in **Figure 3d**), and indicated the rotation directions on the  
275 misorientation profiles (**Figure 4d**). Although the cubic crystal structure of magnetite  
276 complicates the interpretation of the rotation direction, we are able to observe small but  
277 consistent rotation within a magnetite plaquette. In general, magnetite stacks appear to be  
278 comprised of several groups of discs with consistent rotation direction within the group. The  
279 rotation axis is perpendicular to the principal plane of the discs, so that the discs resemble a deck  
280 of cards that rotates about a common axis at the center of the cards (**Figure 5**). Out of the 17  
281 plaquettes we studied by EBSD, the rotation direction appears to be mainly counter-clockwise in  
282 8 plaquettes (following the right-hand rule) and clockwise in 2 plaquettes. The preferred rotation  
283 directions of the rest of the plaquettes are unclear due to the high symmetry of the cubic structure.  
284 The rotational feature resembles the turbostratic feature (non-rational rotation) observed for  
285 graphene layers (Li et al. 2007; Shallcross et al. 2010) and the ‘booklet morphology’ observed  
286 for kaolinite crystallite in diagenetic environments (Meunier 2006). Additional results on the

287 structure and crystallography of magnetite plaquettes collected by transmission electron  
288 microscopy (TEM) analysis will be reported separately.

289

290 In general, the thickness of the magnetite discs ( $\sim 0.2\text{-}0.6\ \mu\text{m}$ ) and the spacing between the edges  
291 of the discs ( $\sim 0.3\text{-}1.0\ \mu\text{m}$ ) are consistent within a given magnetite plaquette. However, magnetite  
292 plaquettes occasionally occur as plate-doublets (**Figure 6**; see Supplementary **Figure S4** for  
293 more images), where the spacing between the edges of the plate-doublet is significantly smaller  
294 than the spacing to the adjacent discs. The magnetization vector can be described by a crystal's  
295 magnetocrystalline anisotropy and therefore corresponds to the orientation of the crystal lattice.  
296 Sheldon and Hoover (2012) proposed that the plate-doublet feature might be related to the  
297 arrangement of discs with alternating aligned and anti-aligned magnetization, so that the spacing  
298 between discs is influenced by the magnetization vector (**Figure 7**). They suggested that the  
299 magnetization state of magnetite plaquettes should be an axially-oriented magnetization shown  
300 in **Figure 7a and b**, as they observed that the small magnetite dipole nanocrystals occurred in  
301 between the edges of the magnetite discs by aligning themselves with the field lines. We have a  
302 different view based on our EBSD observations. Since a plate-doublet is formed by two discs of  
303 different crystal orientations (**Figure 6d**), if the magnetization vector corresponds to crystal  
304 structure, the two magnetite discs in a plate-doublet would have their magnetization orientation  
305 anti-aligned, which is best represented by the scenario outlined in **Figure 7c**, and the discs  
306 immediately adjacent to the plate-doublet would have their magnetization orientation aligned  
307 accordingly (**Figure 7d**). We need further data from magnetic force microscopy/electron  
308 holography to properly interpret the nanoscale magnetic properties of the plaquettes.

309

310 On rare occasions, magnetite plaquettes form an apparent zigzag pattern (**Figure 6b**). Cubic  
311 magnetite only occurs as a single domain (SD) grain when the grain is smaller than  $\sim 0.05 \mu\text{m}$   
312 (Butler and Banerjee 1975; Muxworthy and Williams 2009). Therefore, the magnetite plaquettes  
313 are large enough (diameter  $> 5 \mu\text{m}$ ) to exhibit non-uniform states of magnetization, and thus the  
314 combined effect of the multi-domain magnetization behavior and the rotational feature could  
315 contribute to the observed zigzag pattern. Nevertheless, since the SD size limit of an elongated  
316 magnetite grain can be as large as  $1.4 \mu\text{m}$  (Butler and Banerjee 1975), the platy shaped magnetite  
317 plaquettes should be further studied to visualize the domain structure at the submicron-scale  
318 (Cloete et al. 1999).

319

### 320 **Magnetite plaquettes may influence the formation of organic molecules**

321 The morphology of magnetite plaquettes provides a high surface-area-to-volume ratio for the  
322 adsorption of amino acids, and the subsequent concentration, enantiomeric amplification, and  
323 polymerization into more complex biomolecules. Magnetite would have influenced the chemical  
324 evolution of organic molecules for four reasons. (1) Magnetite has a high abundance in several  
325 classes of CCs, especially those richest in soluble organics. (2) Magnetite has a well-recognized  
326 role in catalyzing the chemical process that produces amino acids (Cronin and Chang 1993;  
327 Pizzarello 2012). Laboratory simulations showed that amino acids could be formed with  
328 magnetite as a catalytic agent (Cronin and Chang 1993; Pizzarello 2012). Therefore, even though  
329 magnetite is not indispensable to the synthesis of amino acids, it probably had a role in  
330 catalyzation of some of the amino acids in asteroidal parent bodies. While magnetite was formed

331 by aqueous alteration and late-stage oxidation of sulfides (Zolensky et al. 2002), concurrent  
332 degradation of organic materials through oxidation could have provided an initial feedstock of  
333 precursor molecules for amino acid synthesis (Cronin and Chang 1993). Magnetite was also  
334 found by infrared reflectance spectroscopy in meteorites showing evidence of adsorbed water  
335 and aliphatic organics (Takir et al. 2013), which again supports a linkage between these  
336 components. (3) The formation of magnetite by aqueous alteration that is known to amplify  
337 amino acid *ee* (Glavin et al. 2011), although the direct influence of aqueous alteration is still  
338 unclear as meteorites showing minimal parent body aqueous alteration also contain abundant  
339 amino acids with significant *ee* (Pizzarello et al. 2012). (4) The availability of a charged surface  
340 for the adsorption and concentration of amino acids through common attraction to surfaces of  
341 opposite charge, which otherwise would not be possible due to electrostatic repulsion (see  
342 Lambert (2008) and references therein).

343

344 Symmetry-breaking mechanisms include processes that can initiate a small *ee* such as selective  
345 adsorption of chiral molecules onto inorganic surfaces (Eckhardt et al. 1993; Lahav and  
346 Leiserowitz 1999; Hazen and Sholl 2003), enantioselective photolysis (Meierhenrich et al. 2005;  
347 Meinert et al. 2012) and phase change such as sublimation (Blackmond and Klusmann 2007;  
348 Viedma et al. 2008; Viedma et al. 2011), which favors further reactions among the molecules of  
349 the adsorbed enantiomer or the remaining enantiomer in solution. Processes such as autocatalytic  
350 processes (Soai et al. 1995) and aqueous alteration (Glavin and Dworkin 2009; Glavin et al.  
351 2012) can then amplify *ee* that has been initiated by the aforementioned symmetry-breaking  
352 processes.

353

354 The ability of inorganic surfaces (e.g., crystalline minerals, chiral mineral surfaces, natural  
355 sediments) to selectively adsorb chiral molecules and the subsequent amplification of their *ee*  
356 have been considered before (Eckhardt et al. 1993; Lahav and Leiserowitz 1999; Hazen and  
357 Sholl 2003; Zaia 2004; Lambert 2008). For instance, about 1.4% asymmetric adsorption of D-  
358 and L-alanine was observed for right- and left-handed quartz, respectively (Soai et al. 1999). Yet,  
359 despite the ability of inorganic surfaces to selectively adsorb chiral molecules, the chiral  
360 preference is not universal. For example, montmorillonite shows a slight preference for the  
361 adsorption of L- over D-glutamic acid, but this trend is opposite for aspartic acid (Siffert and  
362 Naidja 1992). Different crystallographic faces of calcite show different adsorption preferences  
363 for different amino acids (Hazen et al. 2001).

364

365 Magnetite plaquettes were suggested to provide a locally chiral environment that allows  
366 enantioselective adsorption of chiral molecules (Pizzarello and Groy 2011), but the configuration  
367 of such an inorganic/organic interface is unknown. Amino acids were shown to adsorb onto  
368 energetically favorable docking positions on magnetite surfaces where the distances between the  
369 topmost Fe-atoms and the O-atoms of the carboxyl- or carboxylate-group of amino acids are  
370 between 2.6 Å and 4.1 Å (Bürger et al. 2013), and thus the adsorption configuration is controlled  
371 by the atomic arrangement of the magnetite surface structure. The rotational displacement  
372 between the magnetite discs (and thus the corresponding docking positions) might offer an  
373 orientation control of amino acid adsorption/polymerization at the interlayer region at the atomic

374 level. Obviously, further computational and experimental work in this area are necessary to  
375 prove/disprove this hypothesis.

376

377 This proposed symmetry-breaking mechanism does not have to directly result in molecular  
378 homochirality. Chiral initiators usually induce a low *ee*, for example, enantioselective adsorption  
379 of aspartic acid on calcite crystal surfaces was up to 5% *Lee* (Hazen et al. 2001). An  
380 amplification pathway is essential to attain the *ee* observed in meteorites. The initial chiral  
381 asymmetry could further act as organic catalysts, the asymmetry of which could be transferred to  
382 prebiotic organic molecules (Pizzarello and Weber 2004). Isovaline – a nonproteinogenic amino  
383 acid – is commonly used to interpret the extent of meteoritic *ee* since its *Lee* is less influenced by  
384 terrestrial contamination. However, only a handful of isovaline *Lee* data are available in the  
385 literature due to the small isovaline abundance or the lack of chromatographic resolution (e.g.,  
386 Pizzarello et al. 2003; Glavin and Dworkin 2009; Glavin et al. 2011; Burton et al. 2013). Within  
387 the *Lee* data set, some correlation can be drawn between the abundance of magnetite plaquettes  
388 and *Lee* of isovaline. In MET 01070, Mighei, and Tagish Lake, the isovaline *Lee* are between  
389 0.1–7.0%, and these chondrites have only limited occurrence of plaquettes. In contrast,  
390 magnetite plaquettes are abundant in Ivuna, Orgueil and GRO 95577, and the isovaline *Lee* are  
391 between 7.3–15.3% (**Table 2**). However, the correlation between *Lee* and magnetite plaquette  
392 abundance is not universal, for examples, *Lee* was observed to be as high as 18.5% in Murchison,  
393 but no magnetite plaquette was found in our sample. Likewise, a correlation has been observed  
394 for the extent of aqueous alteration and the isovaline *Lee* in meteorites (Glavin and Dworkin  
395 2009), but the trend is not absolute. These exceptions are possibly due to the complex alteration

396 histories which have further magnified the *ee* to different extents, and the heterogeneity between  
397 different meteorite samples used in various studies (e.g., Murchison isovaline *Lee*: 0–18.5%  
398 (Pizzarello et al. 2003; Glavin and Dworkin 2009)).

399

400

### Implications

401 Inorganic surfaces such as chiral mineral surfaces are capable of selectively adsorbing chiral  
402 molecules, and magnetite plaquettes were proposed to be a possible chiral initiator in meteorites  
403 (Pizzarello and Groy 2011). However, as noted by Hazel and Sholl (2003), “*the most pressing*  
404 *current need in this area is to determine accurately the relevant surface structures*”. In this study,  
405 we have shown that magnetite plaquettes are stacks of individual discs based on our SEM and  
406 SXRCT observations. Despite the lack of a spiral feature as assumed in many previous studies,  
407 EBSD offers crystallographic information that substantiates the rotational mechanism of the  
408 plaquettes. In addition to the rotational feature, magnetite nanocrystals have also been found to  
409 be capable of self-assembling into helical superstructures through the interplay between various  
410 nanoscale forces such as van der Waals and magnetic dipole-dipole interactions (Singh et al.  
411 2014). Therefore, magnetite’s inorganic molecular structure and its development into symmetry-  
412 breaking superstructures suggest a possible linkage between magnetism, molecular arrangements,  
413 and symmetry-breaking mechanisms. Our work provides a novel, necessary, and fundamental  
414 understanding of the structure of magnetite plaquettes by revealing its naturally asymmetric  
415 framework.

416

417

## Acknowledgments

418 We acknowledge CAPTEM for loan of the Bench Crater sample, which is an Apollo lunar  
419 sample. We thank Field Museum for Orgueil, Murchison, Mighei, Renazzo, National Museum of  
420 Natural History for the Alais meteorite sample, and American Museum of Natural History for the  
421 Ivuna sample. This study was supported by the NASA Cosmochemistry Program (M.E.Z. is the  
422 PI). Q.H.S.C. acknowledges support from the NASA Postdoctoral Program at the Johnson Space  
423 Center, administered by the Universities Space Research Association. A.T. was supported by a  
424 Grant-in-aid of the Japan Ministry of Education, Culture, Sports, Science and Technology  
425 (15H05695). We thank Tomoki Nakamura, John Bradley, and Rhian Jones for careful reviews of  
426 the manuscript, and Sandra Pizzarello, Jose Aponte, and Aaron Burton for the helpful comments  
427 and insightful discussions. The microtomography experiment was made by the project at SPring-  
428 8 (proposal No. 2015A1413) with help of Kentaro Uesugi and Tsukasa Nakano.

429

430

## References

- 431 Bennett, C., Graham, J., and Thornber, M. (1972) New observations on natural pyrrhotites Part I.  
432 Mineragraphic techniques. *Mineragraphic techniques: American Mineralogist*, 57, 445-  
433 462.
- 434 Blackmond, D.G., and Klusmann, M. (2007) Spoilt for choice: assessing phase behavior models  
435 for the evolution of homochirality. *Chemical Communications*(39), 3990-3996.
- 436 Botta, O., Glavin, D.P., Kminek, G., and Bada, J.L. (2002) Relative amino acid concentrations as  
437 a signature for parent body processes of carbonaceous chondrites. *Origins of life and*  
438 *evolution of the biosphere*, 32(2), 143–163.
- 439 Bradley, J.P., McSween, H.Y., and Harvey, R.P. (1998) Epitaxial growth of nanophase  
440 magnetite in Martian meteorite Allan Hills 84001: Implications for biogenic  
441 mineralization. *Meteoritics & Planetary Science*, 33(4), 765-773.
- 442 Bürger, A., Magdans, U., and Gies, H. (2013) Adsorption of amino acids on the magnetite-(111)-  
443 surface: a force field study. *Journal of Molecular Modeling*, 19(2), 851-857.
- 444 Burton, A.S., Elsila, J.E., Hein, J.E., Glavin, D.P., and Dworkin, J.P. (2013) Extraterrestrial  
445 amino acids identified in metal-rich CH and CB carbonaceous chondrites from Antarctica.  
446 *Meteoritics & Planetary Science*, 48(3), 390-402.
- 447 Burton, A.S., Grunsfeld, S., Elsila, J.E., Glavin, D.P., and Dworkin, J.P. (2014) The effects of  
448 parent-body hydrothermal heating on amino acid abundances in CI-like chondrites. *Polar*  
449 *Science*, 8(3), 255-263.

- 450 Burton, A.S., Stern, J.C., Elsila, J.E., Glavin, D.P., and Dworkin, J.P. (2012) Understanding  
451 prebiotic chemistry through the analysis of extraterrestrial amino acids and nucleobases  
452 in meteorites. *Chemical Society Reviews*, 41(16), 5459-5472.
- 453 Butler, R.F., and Banerjee, S.K. (1975) Theoretical single-domain grain size range in magnetite  
454 and titanomagnetite. *Journal of Geophysical Research*, 80(29), 4049-4058.
- 455 Cloete, M., Hart, R.J., Schmid, H.K., Drury, M., Demanet, C.M., and Sankar, K.V. (1999)  
456 Characterization of magnetite particles in shocked quartz by means of electron- and  
457 magnetic force microscopy: Vredefort, South Africa. *Contributions to Mineralogy and  
458 Petrology*, 137(3), 232-245.
- 459 Cronin, J.R., and Chang, S. (1993) Organic matter in meteorites: molecular and isotopic analyses  
460 of the Murchison meteorite. In J.M. Greenberg, C.X. Mendoza-Gomez, and V. Pirronello,  
461 Eds. *NATO ASIC Proc. 416: The Chemistry of Life's Origins*.
- 462 Eckhardt, C.J., Peachey, N.M., Swanson, D.R., Takacs, J.M., Khan, M.A., Gong, X., Kim, J.H.,  
463 Wang, J., and Uphaus, R.A. (1993) Separation of chiral phases in monolayer crystals of  
464 racemic amphiphiles. *Nature*, 362(6421), 614-616.
- 465 Frank, F.C. (1949) The influence of dislocations on crystal growth. *Discussions of the Faraday  
466 Society*, 5(0), 48-54.
- 467 Glavin, D.P., Callahan, M.P., Dworkin, J.P., and Elsila, J.E. (2011) The effects of parent body  
468 processes on amino acids in carbonaceous chondrites. *Meteoritics & Planetary Science*,  
469 45(12), 1948-1972.
- 470 Glavin, D.P., and Dworkin, J.P. (2009) Enrichment of the amino acid L-isovaline by aqueous  
471 alteration on CI and CM meteorite parent bodies. *PNAS*, 106(14), 5487-5492.

- 472 Glavin, D.P., Elsila, J.E., Burton, A.S., Callahan, M.P., Dworkin, J.P., Hilts, R.W., and Herd,  
473 C.D.K. (2012) Unusual nonterrestrial l-proteinogenic amino acid excesses in the Tagish  
474 Lake meteorite. *Meteoritics & Planetary Science*, 47(8), 1347-1364.
- 475 Greshake, A., Krot, A.N., Flynn, G.J., and Keil, K. (2005) Fine-grained dust rims in the Tagish  
476 Lake carbonaceous chondrite: Evidence for parent body alteration. *Meteoritics &*  
477 *Planetary Science*, 40(9-10), 1413-1431.
- 478 Hazen, R.M., Filley, T.R., and Goodfriend, G.A. (2001) Selective adsorption of l- and d-amino  
479 acids on calcite: Implications for biochemical homochirality. *Proceedings of the National*  
480 *Academy of Sciences*, 98(10), 5487-5490.
- 481 Hazen, R.M., and Sholl, D.S. (2003) Chiral selection on inorganic crystalline surfaces. *Nat Mater*,  
482 2(6), 367-374.
- 483 Hua, X., and Buseck, P.R. (1998) Unusual forms of magnetite in the Orgueil carbonaceous  
484 chondrite. *Meteoritics & Planetary Science*, 33(S4), A215-A220.
- 485 Izawa, M.R.M., Flemming, R.L., McCausland, P.J.A., Southam, G., Moser, D.E., and Barker,  
486 I.R. (2010) Multi-technique investigation reveals new mineral, chemical, and textural  
487 heterogeneity in the Tagish Lake C2 chondrite. *Planetary and Space Science*, 58(10),  
488 1347-1364.
- 489 Jedwab, J. (1967) La magnetite en plaquettes des meteorites carbonees d'alais, ivuna et orgueil.  
490 *Earth and Planetary Science Letters*, 2(5), 440-444.
- 491 -. (1971) La magnétite de la météorite d'Orgueil vue au microscope électronique à balayage.  
492 *Icarus*, 15(2), 319-340.

- 493 Keller, L.P., McKeegan, K., and Sharp, Z. (2012) The oxygen isotopic composition of MIL  
494 090001: a CR2 chondrite with abundant refractory inclusions.
- 495 Keller, L.P., and Walker, R.M. (2011) Mineralogy and petrography of MIL 090001, a highly  
496 altered CV chondrite from the reduced sub-group. 42nd Lunar and Planetary Institute  
497 Science Conference, 42, p. 2409.
- 498 Kereszturi, A., Blumberger, Z., Józsa, S., May, Z., Müller, A., Szabó, M., and Tóth, M. (2014)  
499 Alteration processes in the CV chondrite parent body based on analysis of NWA 2086  
500 meteorite. *Meteoritics & Planetary Science*, 49(8), 1350-1364.
- 501 Kerridge, J.F., Mackay, A.L., and Boynton, W.V. (1979) Magnetite in CI carbonaceous  
502 meteorites: Origin by aqueous activity on a planetesimal surface. *Science*, 205(4404),  
503 395-397.
- 504 Lahav, M., and Leiserowitz, L. (1999) Spontaneous Resolution: From Three-Dimensional  
505 Crystals to Two-Dimensional Magic Nanoclusters. *Angewandte Chemie International  
506 Edition*, 38(17), 2533-2536.
- 507 Lambert, J.-F. (2008) Adsorption and Polymerization of Amino Acids on Mineral Surfaces: A  
508 Review. *Origins of Life and Evolution of Biospheres*, 38(3), 211-242.
- 509 Li, Z.Q., Lu, C.J., Xia, Z.P., Zhou, Y., and Luo, Z. (2007) X-ray diffraction patterns of graphite  
510 and turbostratic carbon. *Carbon*, 45(8), 1686-1695.
- 511 Lipschutz, M.E., Zolensky, M.E., and Bell, M.S. (1999) New petrographic and trace element  
512 data on thermally metamorphosed carbonaceous chondrites. *Antarctic meteorite research*,  
513 12, 57.

- 514 Meierhenrich, U.J., Nahon, L., Alcaraz, C., Bredehöft, J.H., Hoffmann, S.V., Barbier, B., and  
515 Brack, A. (2005) Asymmetric Vacuum UV photolysis of the Amino Acid Leucine in the  
516 Solid State. *Angewandte Chemie International Edition*, 44(35), 5630-5634.
- 517 Meinert, C., Bredehöft, J.H., Filippi, J.-J., Baraud, Y., Nahon, L., Wien, F., Jones, N.C.,  
518 Hoffmann, S.V., and Meierhenrich, U.J. (2012) Anisotropy Spectra of Amino Acids.  
519 *Angewandte Chemie International Edition*, 51(18), 4484-4487.
- 520 Meunier, A. (2006) Why are clay minerals small? *Clay Minerals*, 41(2), 551-566.
- 521 Muxworthy, A.R., and Williams, W. (2009) Critical superparamagnetic/single-domain grain  
522 sizes in interacting magnetite particles: implications for magnetosome crystals. *Journal of*  
523 *the Royal Society Interface*, 6(41), 1207-1212.
- 524 Pizzarello, S. (2012) Catalytic syntheses of amino acids and their significance for nebular and  
525 planetary chemistry. *Meteoritics & Planetary Science*, 47(8), 1291-1296.
- 526 Pizzarello, S., and Groy, T.L. (2011) Molecular asymmetry in extraterrestrial organic chemistry:  
527 An analytical perspective. *Geochimica et Cosmochimica Acta*, 75(2), 645-656.
- 528 Pizzarello, S., Schrader, D.L., Monroe, A.A., and Lauretta, D.S. (2012) Large enantiomeric  
529 excesses in primitive meteorites and the diverse effects of water in cosmochemical  
530 evolution. *Proceedings of the National Academy of Sciences of the United States of*  
531 *America*, 109(30), 11949-11954.
- 532 Pizzarello, S., and Weber, A.L. (2004) Prebiotic Amino Acids as Asymmetric Catalysts. *Science*,  
533 303(5661), 1151.

- 534 Pizzarello, S., Zolensky, M., and Turk, K.A. (2003) Nonracemic isovaline in the Murchison  
535 meteorite: Chiral distribution and mineral association. *Geochimica et Cosmochimica*  
536 *Acta*, 67(8), 1589-1595.
- 537 Shallcross, S., Sharma, S., Kandelaki, E., and Pankratov, O.A. (2010) Electronic structure of  
538 turbostratic graphene. *Physical Review B*, 81(16), 165105.
- 539 Sheldon, R.B., and Hoover, R. (2012) Carbonaceous chondrites as bioengineered comets. *SPIE*  
540 *Optical Engineering+ Applications*, p. 85210N-85210N-16. International Society for  
541 Optics and Photonics.
- 542 Siffert, B., and Naidja, A. (1992) Stereoselectivity of montmorillonite in the adsorption and  
543 deamination of some amino acids. *Clay Minerals*, 27(1), 109-118.
- 544 Singh, G., Chan, H., Baskin, A., Gelman, E., Repnin, N., Král, P., and Klajn, R. (2014) Self-  
545 assembly of magnetite nanocubes into helical superstructures. *Science*, 345(6201), 1149-  
546 1153.
- 547 Soai, K., Osanai, S., Kadowaki, K., Yonekubo, S., Shibata, T., and Sato, I. (1999) d- and l-  
548 Quartz-Promoted Highly Enantioselective Synthesis of a Chiral Organic Compound.  
549 *Journal of the American Chemical Society*, 121(48), 11235-11236.
- 550 Soai, K., Shibata, T., Morioka, H., and Choji, K. (1995) Asymmetric autocatalysis and  
551 amplification of enantiomeric excess of a chiral molecule. *Nature*, 378(6559), 767-768.
- 552 Sugiura, N. (2000) Petrographic evidence for in-situ hydration of the CH chondrite PCA91467.  
553 *Lunar and Planetary Institute Science Conference Abstracts*, 31, p. 1503.

- 554 Takir, D., Emery, J.P., McSween, H.Y., Hibbitts, C.A., Clark, R.N., Pearson, N., and Wang, A.  
555 (2013) Nature and degree of aqueous alteration in CM and CI carbonaceous chondrites.  
556 *Meteoritics & Planetary Science*, 48(9), 1618-1637.
- 557 Trigo-Rodriquez, J., Moyano-Camero, C., Mestres, N., Fraxedas, J., Zolensky, M., Nakamura,  
558 T., and Martins, Z. (2013) Evidence for extended aqueous alteration in CR carbonaceous  
559 chondrites.
- 560 Tsuchiyama, A., Nakano, T., Uesugi, K., Uesugi, M., Takeuchi, A., Suzuki, Y., Noguchi, R.,  
561 Matsumoto, T., Matsuno, J., Nagano, T., Imai, Y., Nakamura, T., Ogami, T., Noguchi, T.,  
562 Abe, M., Yada, T., and Fujimura, A. (2013) Analytical dual-energy microtomography: A  
563 new method for obtaining three-dimensional mineral phase images and its application to  
564 Hayabusa samples. *Geochimica et Cosmochimica Acta*, 116, 5-16.
- 565 Viedma, C., Noorduyn, W.L., Ortiz, J.E., Torres, T.d., and Cintas, P. (2011) Asymmetric  
566 amplification in amino acid sublimation involving racemic compound to conglomerate  
567 conversion. *Chemical Communications*, 47(2), 671-673.
- 568 Viedma, C., Ortiz, J.E., Torres, T.d., Izumi, T., and Blackmond, D.G. (2008) Evolution of Solid  
569 Phase Homochirality for a Proteinogenic Amino Acid. *Journal of the American Chemical*  
570 *Society*, 130(46), 15274-15275.
- 571 Weisberg, M.K., Prinz, M., Clayton, R.N., and Mayeda, T.K. (1993) The CR (Renazzo-type)  
572 carbonaceous chondrite group and its implications. *Geochimica et Cosmochimica Acta*,  
573 57(7), 1567-1586.
- 574 Yao, N., Epstein, A.K., Liu, W.W., Sauer, F., and Yang, N. (2009) Organic–inorganic interfaces  
575 and spiral growth in nacre. *Journal of The Royal Society Interface*, 6(33), 367-376.

- 576 Zaia, D.A.M. (2004) A review of adsorption of amino acids on minerals: Was it important for  
577 origin of life? *Amino Acids*, 27(1), 113-118.
- 578 Zolensky, M.E., Ivanov, A.V., Yang, S.V., Mittlefehldt, D.W., and Ohsumi, K. (1996a) The  
579 Kaidun meteorite: Mineralogy of an unusual CM1 lithology. *Meteoritics & Planetary*  
580 *Science*, 31(4), 484-493.
- 581 Zolensky, M.E., Nakamura, K., Gounelle, M., Mikouchi, T., Kasama, T., Tachikawa, O., and  
582 Tonui, E. (2002) Mineralogy of Tagish Lake: An ungrouped type 2 carbonaceous  
583 chondrite. *Meteoritics & Planetary Science*, 37(5), 737-761.
- 584 Zolensky, M.E., Weisberg, M.K., Buchanan, P.C., and Mittlefehldt, D.W. (1996b) Mineralogy of  
585 carbonaceous chondrite clasts in HED achondrites and the Moon. *Meteoritics &*  
586 *Planetary Science*, 31(4), 518-537.
- 587
- 588
- 589

590

### List of figure captions

591 **Figure 1. BSE images of selected magnetite plaquettes observed in the CC samples. a, A**  
592 cluster of magnetite plaquettes in Orgueil; some carbonate materials (c) are marked. **b, Abundant**  
593 magnetite plaquettes were found within a healed fracture in Orgueil. **c, Spiral-like features of a**  
594 magnetite plaquette in Orgueil hosted in a phyllosilicate matrix. **d, Non-spiral like features of a**  
595 magnetite plaquette in Orgueil; Note the association of framboidal magnetite grains around the  
596 plaquette; arrow marks the edge of a large magnetite spherule that displays radiating structure.

597

598 **Figure 2. The three-dimensional shape of a selected magnetite plaquettes in Orgueil. A,**  
599 Slice images of the FIB section. Arrow indicates the location of the plaquettes selected for CT. **b,**  
600 The final compiled three-dimensional structure of the selected plaquette obtained by stacking  
601 successive CT images as viewed from four different directions. The images show that the  
602 plaquette is composed of discs that do not join together as a spiral. Instead they occur as  
603 individual parallel discs, each with a solid center.

604

605 **Figure 3. EBSD pattern and the calculated crystal orientation. a, Observed EBSD pattern. b,**  
606 Matching EBSD pattern. **c, Calculated EBSD pattern. d, Crystal structure of magnetite Fe<sub>3</sub>O<sub>4</sub>**  
607 oriented according to the extrapolated crystal orientation. The location of the analyzed spot is  
608 indicated by the yellow crosses in **Figure 4a and b.**

609

610 **Figure 4. SEM BSE image and EBSD data of magnetite plaquettes in Orgueil. a, BSE image**  
611 of the selected plaquettes. The location of the analyzed spot shown in **Figure 3** is indicated by a

612 yellow cross; **b**, IPF map of the selected plaquettes. IPF map legend indicates crystal orientation.  
613 Grains with their [001], [101] or [111] axes parallel to the sample projection direction of the IPF  
614 map (IPFX, normal to the rolling direction) are represented by red, green and blue colors  
615 respectively. Misorientation profiles were obtained for the grains along the Lines A-A'' and B-  
616 B''; **c**, Graph showing the change in crystal orientation along Line A-A''. The misorientation  
617 angle was calculated with respect to the crystal orientation of the initial point (i.e. Point A). The  
618 location of the analyzed spot shown in **Figure 3** is indicated by a yellow cross; **d**, Graph showing  
619 the change in crystal orientation along Line B-B''. The misorientation angle was calculated with  
620 respect to the crystal orientation of previous points along the profile. Rotation directions are  
621 indicated with (L) and (D) for clockwise and counter-clockwise rotation respectively. (?) denotes  
622 abrupt changes in crystal orientation of which the directions do not conform to the arbitrary  
623 rotational axis.

624

625 **Figure 5. A schematic representation of the magnetite rotation feature. a**, A view of the  
626 rotation feature from the top. The dot in the center marks the location of the rotation axis. The  
627 red arrow indicates right-handed rotation orientation (counter-clockwise) following the right-  
628 hand rule. Different groups of discs with consistent rotation direction are represented by  
629 alternating colors; **b**, A view from the side of the rotation feature with the same configuration as  
630 **Figure 5a**.

631

632 **Figure 6. BSE images and IPF map of magnetite plate-doublers. a**, A magnetite plaquette in  
633 Ivuna showing plate-doublers. **b**, A magnetite plaquette in PCA 91467 showing an apparent

634 zigzag pattern. The more prominent part of the zigzag pattern is highlighted in the blue box. **c**,  
635 Another magnetite plaquette in Orgueil showing the plate-doublets, the boundaries between the  
636 doublets are marked by dotted lines. **d**, An IPF map of the magnetite plaquette shown in **c**. Note  
637 that the discs within a plate-doublet have different crystal orientations, but they share the same  
638 crystal orientation with the corresponding adjacent disc.

639

640 **Figure 7. Four magnetization schemes that form magnetite plate-doublets. a**, Axially-  
641 oriented and aligned; **b**, Axially-oriented and anti-aligned; **c**, Diametrically-oriented and anti-  
642 aligned; **d**, Diametrically-oriented and aligned.

643

644

645

**Tables**

646 **Table 1. Measurements describing the geometry of the magnetite plaquettes.**

Meteorite		Magnetite plaquettes					No. of discs	Reference
		Occurrence	Stack thickness <sup>1</sup>	Disc diameter <sup>2</sup>	Disc thickness <sup>3</sup>	Ridge spacing <sup>4</sup>		
CI1	Alais	Observed	6.4	15.6	0.63	1.01	8	This study
	Ivuna	Observed	6.9	7.9	0.34	0.35	20	This study
	Orgueil	Observed	7.2	13.2	0.40	0.43	15	This study
CM1	MET 01070	No	--	--	--	--	--	This study
	LAP 02422	Observed	6.6	5.7	0.25	0.32	22	This study
CM2	Murchison	No	--	--	--	--	--	This study
	Mighei	No	--	--	--	--	--	This study
CO3	ALHA77307	No	--	--	--	--	--	This study
CV3	NWA 2086	No	--	--	--	--	--	This study
CR1	GRO 95577	Observed	4.5	7.3	0.34	0.47	8	This study
CR2	GRA 95229	Observed	3.6	7.8	0.28	0.37	4	This study
	Renazzo	Observed	6.6	7.1	0.55	0.56	13	This study
CH3	PCA 91467	Observed	5.8	9.0	0.26	0.41	16	This study
CM1	Bench Crater	Observed	9.2	6.8	0.40	0.75	17	This study
C2	Tagish Lake	(Literature)	7.8	7.3	0.19	0.28	24	Zolensky et al. 2002

<sup>1</sup>Thickness (μm) of the largest measurable magnetite stack identified.

<sup>2</sup>Diameter (μm) of the largest disc in the same magnetite stack.

<sup>3</sup>Thickness (μm) of the thickest disc in the same magnetite stack.

<sup>4</sup>Spacing (μm) between the ridges of two discs in the same magnetite stack.

647

648 **Table 2. Comparison between the abundances of magnetite plaquettes and isovaline enantiomeric excesses in the studied**  
 649 **carbonaceous chondrites.**

	Meteorite	Plaquette abundance	Isovaline Lee (%) <sup>a</sup>	Isovaline abundance (ppb) <sup>a</sup>
CI1	Alais	●●●	b	b
	Ivuna	●●●	7.3	48 ± 25
	Orgueil	●●●	15.3 ± 4.0	85 ± 4
CR1	GRO 95577	●●	11.0	33 ± 3
CR2	GRA 95229	●●	c	29,245 ± 2,229
	Renazzo	●●	c	349 ± 33
CM1	MET 01070		0.1	<0.9
	LAP 02422	●	b	b
	Bench Crater	●	b	b
CM2	Murchison		0–18.5	2,437 ± 79
	Mighei		7.8	295 ± 145
CO3	ALHA77307		<1	<0.2
CV3	NWA 2086		b	b
CH3	PCA 91467	●	13.0 ± 3.0	92 ± 8
C2	Tagish Lake	●	7.0 ± 1.9	14 ± 0

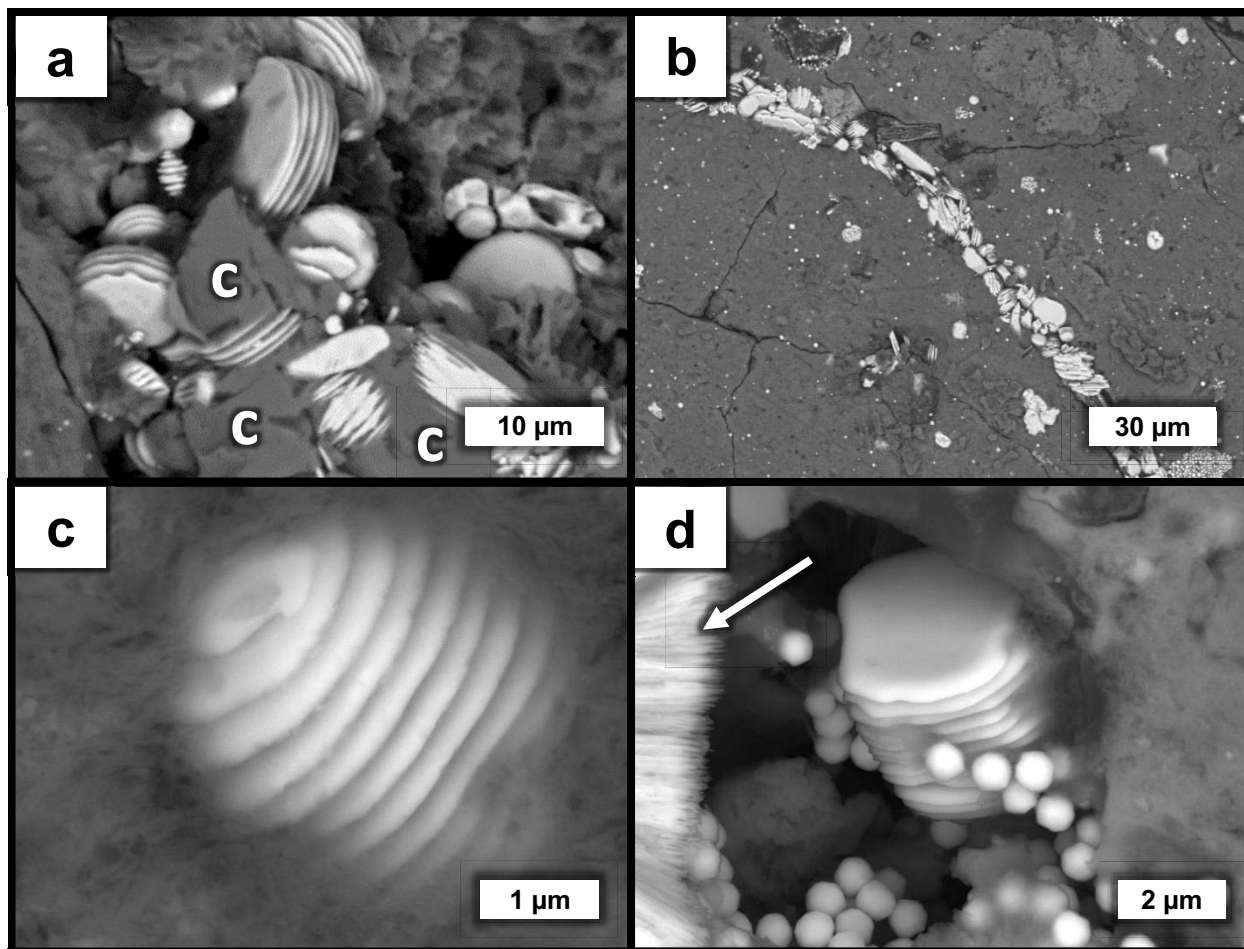
<sup>a</sup>Lee (%) = (L – D)/(L + D) × 100. Lee data from Burton et al. (2012; 2013; 2014); Botta et al. (2002); Glavin and Dworkin (2009); Glavin et al. (2011; 2012); Pizzarello et al. (2003)

<sup>b</sup>No available data.

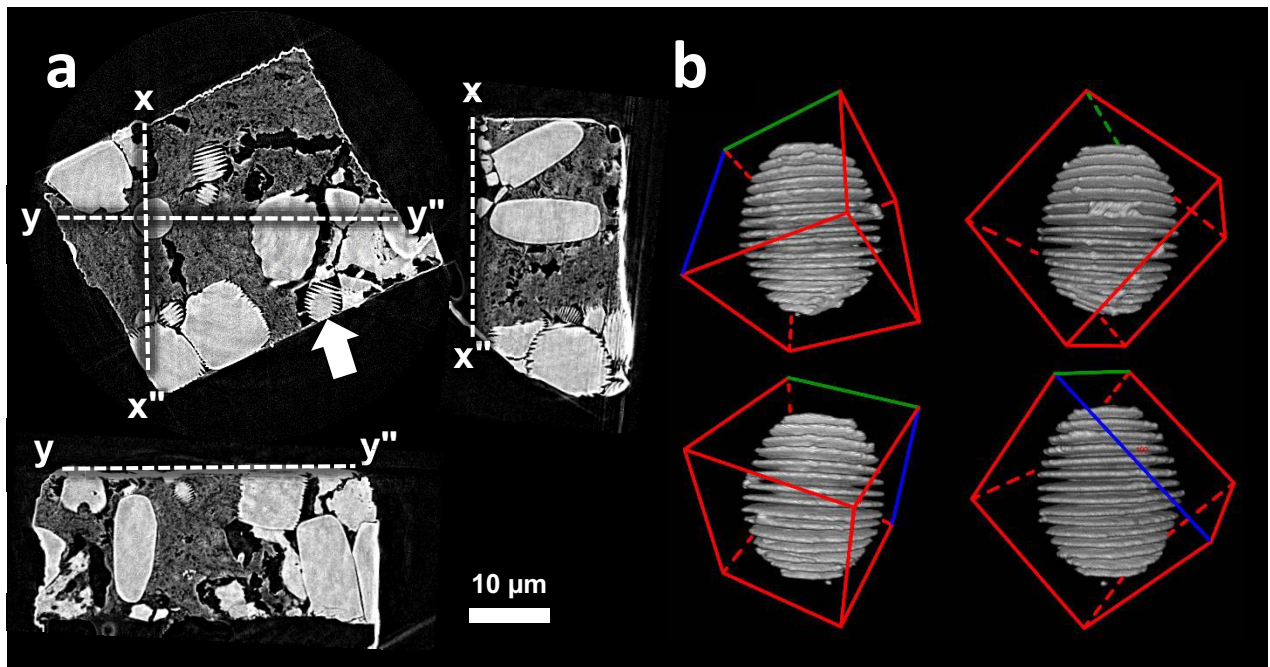
<sup>c</sup>Enantiomers could not be separated under the chromatographic conditions

650

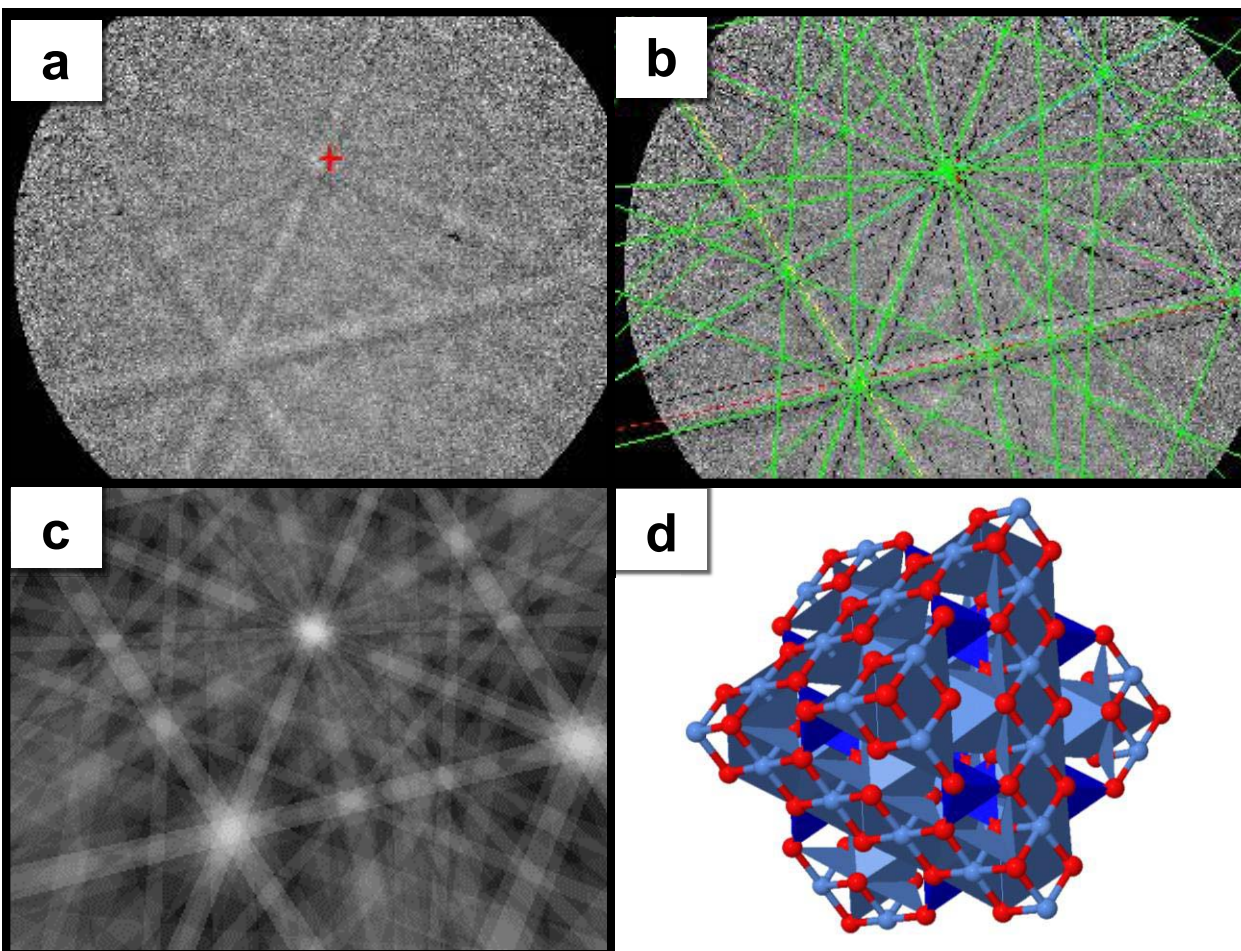
Chan et al. 2016  
**Manuscript - Figure 1**



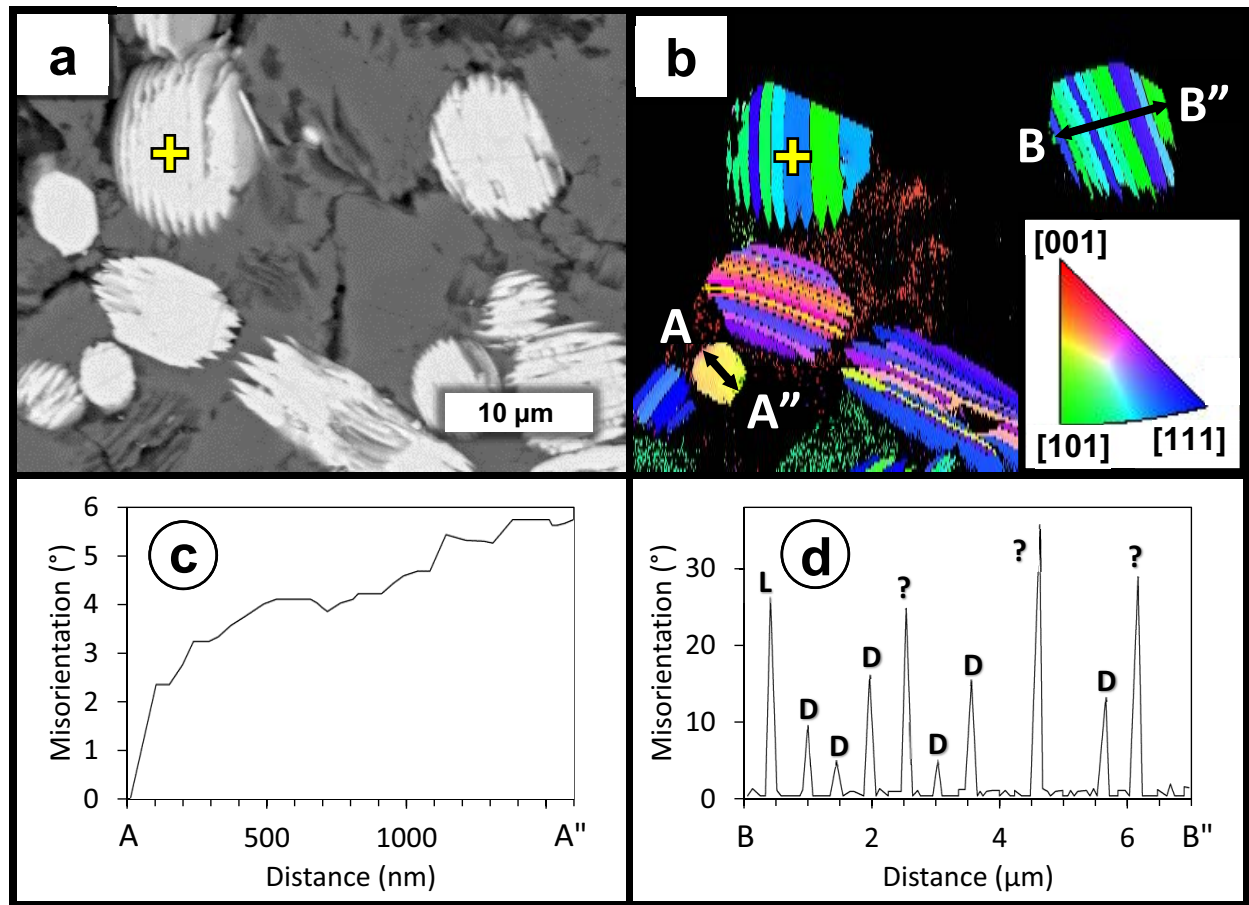
Chan et al. 2016  
Manuscript - Figure 2



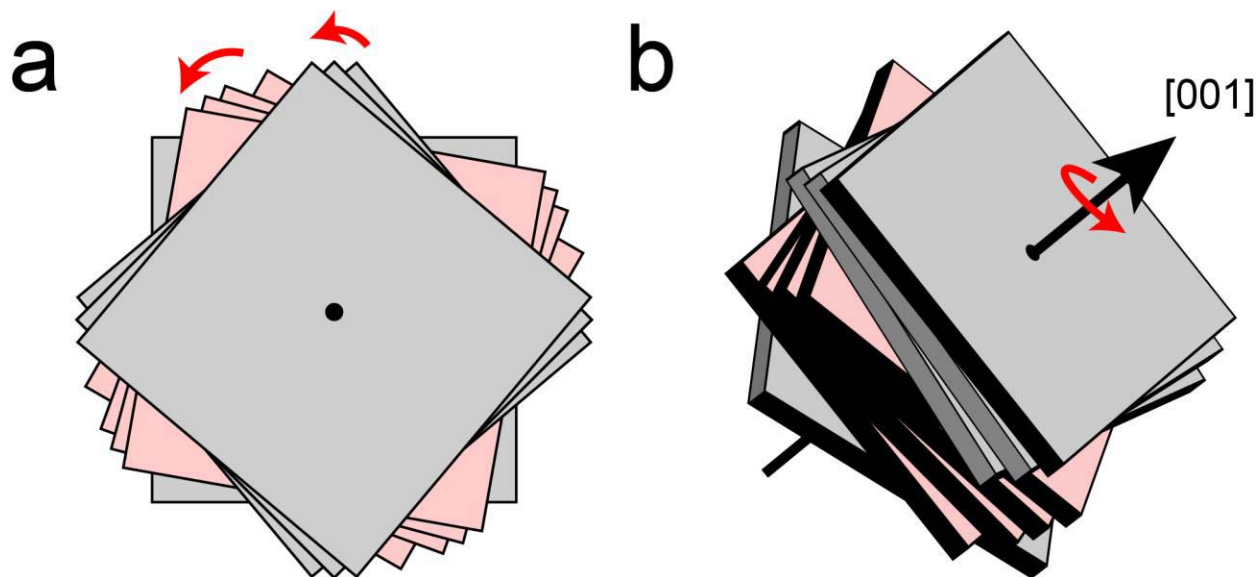
Chan et al. 2016  
Manuscript - Figure 3



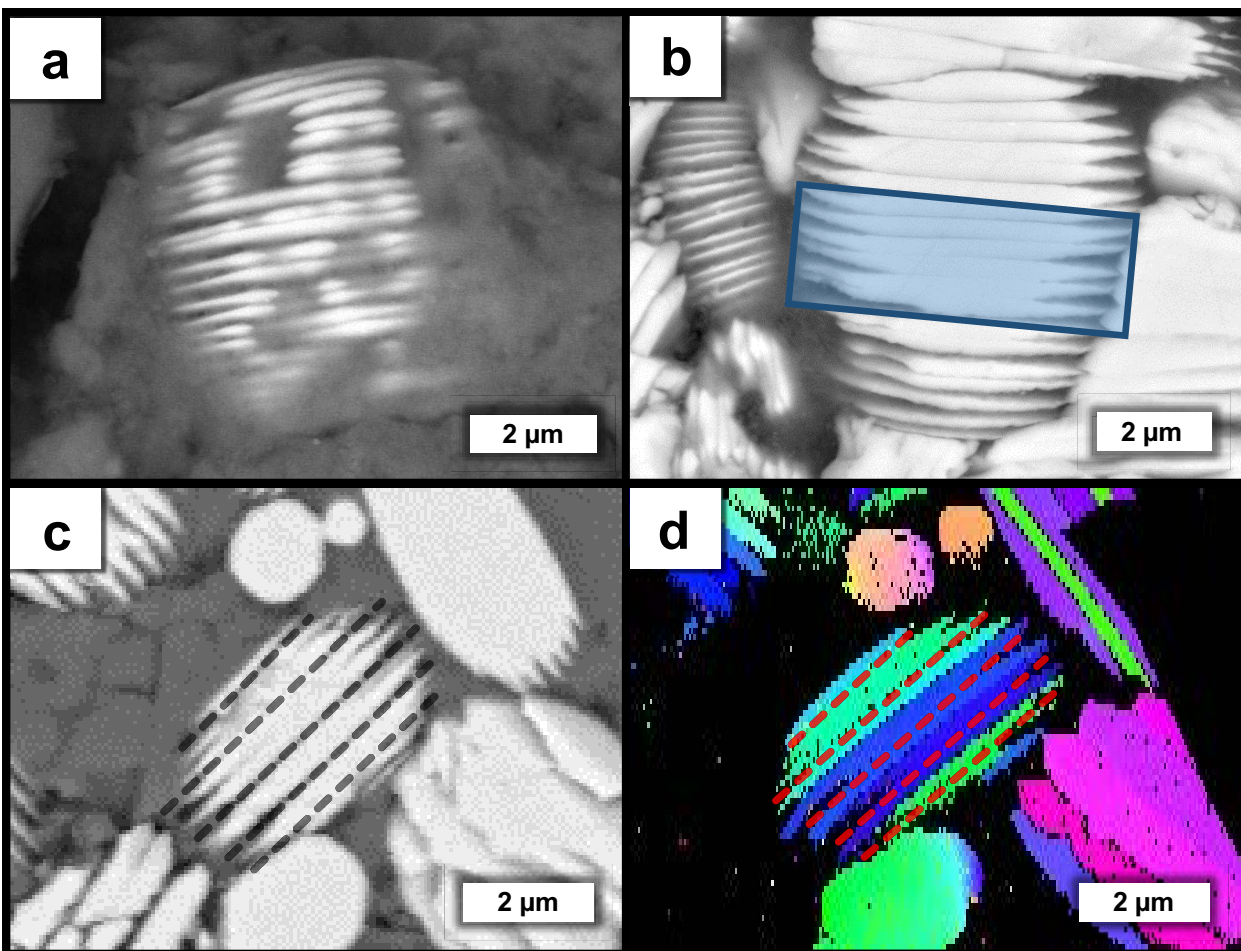
Chan et al. 2016  
Manuscript - Figure 4



Chan et al. 2016  
Manuscript - Figure 5



Chan et al. 2016  
Manuscript - Figure 6



Chan et al. 2016  
**Manuscript - Figure 7**

